ARMA 19–1757

DEM models to predict side shear resistance of rock-socketed piles considering socket roughness

Gutiérrez-Ch, J.G.
Universidad Politécnica de Madrid, Madrid, Spain
Melentijevic, S.
Universidad Complutense de Madrid, Madrid, Spain
Senent, S. and Jimenez, R.
Universidad Politécnica de Madrid, Madrid, Spain

This paper was prepared for presentation at the 53rd US Rock Mechanics/Geomechanics Symposium held in New York, NY, USA, 23–26 June 2019. This paper was selected for presentation at the symposium by an ARMA Technical Program Committee based on a technical and critical review of the paper by a minimum of two technical reviewers. The material, as presented, does not necessarily reflect any position of ARMA, its officers, or members. Electronic reproduction, distribution, or storage of any part of this paper for commercial purposes without the written consent of ARMA is prohibited. Permission to reproduce in print is restricted to an abstract of not more than 200 words; illustrations may not be copied. The abstract must contain conspicuous acknowledgement of where and by whom the paper was presented.

ABSTRACT: Rock-socketed piles are designed to receive and transmit large concentrated loads to deeper stronger materials. Although the load transfer mechanism combines base and side resistances, the side shear resistance is usually mobilized at much lower strains than base resistance. The side shear resistance of rock-socketed piles has usually been estimated using recommendations from codes and standards, or using local knowledge obtained from load tests performed in similar ground. There are also empirical formulations as a function of the uniaxial compressive strength of the intact rock (UCS). However, this approach neglects the influence of other important aspects such as the roughness at the pile-rock interface. This work examines the socket roughness effect on side shear resistance of rock-socketed piles, using DEM^{3D} numerical models of rock-socketed piles with different degrees of socket roughness. Numerical results suggest that socket roughness is an important factor that significantly increases the load capacity and stiffness of rock-socketed piles. Finally, a new approach to predict preliminary the average side shear resistance of rock-sockets is analysed, considering the socket roughness and the UCS of the intact weaker material (rock or pile).

1. INTRODUCTION

Rock-socketed piles loaded axially might transfer the working load by the combination of base and side shear resistance, or only by base or by side shear resistance. The situations in which the piles could carry out their working load by side shear resistance only are diverse (e.g., the base hole cleaning is not guaranteed or the drilled hole was made in rocks with cavities) (Seidel and Collingwood, 2001). On the other hand, when the bottom pile is on a high strength rock and an overlying low strength rock exists, base resistance only can be assumed; however, if the piles are socketed in rocks at greater depths, both situations might be presented but the side shear resistance is usually mobilized first for lower pile settlements (Zhang, 2004).

Traditionally the side shear resistance design of rock-socketed piles is based on state codes and standards or local knowledge obtained from full-scale static load tests performed in similar ground (Seidel and Collingwood, 2001), but also on empirical correlations using the uniaxial compressive strength (UCS or σ_c) (Rezazadeh and Eslani, 2017). The form of these empirical criteria can be generalized as:

$$f_{ave,peak} = \alpha {\sigma_c}^{\beta} \quad (1)$$

where $f_{ave,peak}$ is the average ultimate side shear resistance, σ_c is the intact UCS of the weaker of the materials involved at the shear surface (rock or pile), and α and β are empirical factors that depend on the type of rock, or in some cases on the roughness (Seo et al. 2013). However, O'Neill et al. (1996) after their analysis and interpretation of 245 load tests in different types of materials, suggested that other parameters in addition to σ_c are required for a good estimation of $f_{ave,peak}$.

As a result of several investigations, it is well known that the main factors affecting the side shear resistance are: the drilling construction method (O'Neill et al. 1996) and drilling tools used (Nam and Vipulanandan, 2008), the type and quality of the rock mass (Haberfield, 2013; Melentijevic and Olalla, 2014), the depth and diameter of the socket (Seidel and Haberfield, 1995; Seol and Jeong, 2007), the residual drilling fluid coating the socket walls and thickness of smear zone (Williams and Pells, 1981; Haberfield, 2013), but also the initial normal stress and roughness at the pile-rock interface (Pells et al. 1980; Seidel and Collingwood, 2001).

This paper focuses on the influence of roughness at the pile-rock interface on the side shear resistance of rock-socketed piles. In particular, this research analizes the applicability of DEM to model rock-socketed piles with PFC^{3D} and proposes a factor $\alpha_{RF,0.01D}$ to predict side shear resistance considering socket roughness and the uniaxial compressive strength of the intact weaker material (rock or pile).

2. FUNDAMENTALS OF DEM MODELLING WITH PFC

Particle Flow Code (PFC) is the commercial software (Itasca Consulting Group Inc., 2014) with Distinct Element Method (DEM) implementation employed in this work. In PFC model, the movements and interactions of systems composed of rigid and finite-sized particles –circular (PFC^{2D}) or spherical (PFC^{3D}) with a uniform or Gaussian distribution– can be simulated. Mechanical interactions are created or destroyed by the contact-detection logic whenever bodies are sufficiently close or separated. Particles interact through pair-wise contacts with internal forces and moments. In addition to particles, PFC models include walls to apply velocity boundary conditions to assemblies of particles, but also for compaction and confinement. The walls and particles interact with one another through the forces that arise at contacts. The system evolution is computed by DEM schemes, through explicit dynamic simulation of Newton's second law to the particles and a force-displacement law at the contacts (Itasca Consulting Group Inc., 2014).

PFC provides a Bonded-Particle Model (BPM) (Potyondy, 2015) to simulate cohesive or bonded material (e.g., concrete or rock) with several possible contact models; it also provides "interfaces" among materials to characterize their behaviour when they are in contact. In this work, the Flat-Joint Contact Model (FJCM) –to reproduce 3D pile and rock bodies involved in the tests–, and the Smooth-Joint Contact Model (SJCM) –to simulate the behaviour at the pile-rock interface–, are employed.

The FJCM simulates the contact between particles in the BPM using locally notional (bonded or unbonded) surfaces (see Fig. 1), which are discretized into elements (Potyondy, 2012); while the SJCM reproduces the macroscopic behaviour of a interface (bonded or unbonded) formed by several particles, in which particles are allowed to overlap or slide past each other, instead of being forced to move around one another (see Fig. 2). Additional details of both models are available in Potyondy, 2015; Ivars et al., 2008; and Itasca Consulting Group Inc., 2014.

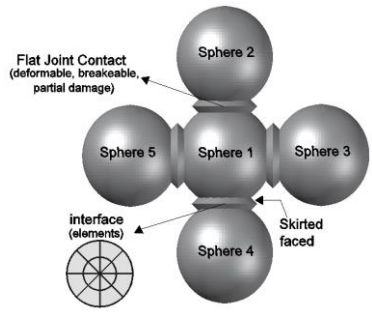

Fig. 1. Idealization of flat joint material (modified from Itasca Consulting Group Inc., 2014).

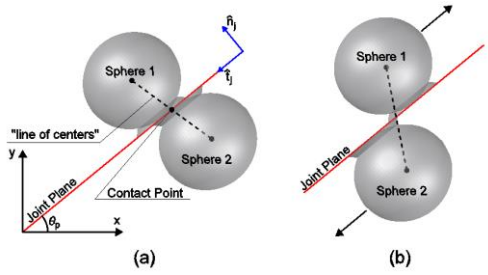

Fig. 2. Effective joint geometry: (a) notation used to define joint and smooth-joint contacts, (b) physical analogue of Smooth-Joint Contact Model (modified from Ivars et al., 2011).

3. NUMERICAL SIMULATION OF ROCK-SOCKETED PILES USING DEM^{3D}

3.1. Calibration of the microparameters

To employ the DEM models, the micromechanical parameters of the materials –i.e., rock and concrete– and of the rock-concrete interfaces should be calibrated first. To validate de calibration process, the uniaxial compression tests and direct shear tests conducted by Gu et al. (2003) on sandstone and concrete samples, are employed.

Usually, the micromechanical parameters of the FJCM employed for intact materials have been calibrated using the uniaxial compressive strength (UCS) test –i.e., the comparison between DEM and laboratory tests results– (Bahaaddini et al., 2014; Castro-Filgueira et al., 2017). In this work, the methodology proposed by Gutiérrez-Ch et al. (2018) is used. The procedure starts matching the macroscopic Poisson's ratio (ν), which mainly depends on the particle and flat-joint normal-to-shear stiffness ratios (k^* and $\overline{k^*}$) Next, the macroscopic Young's modulus (E), is calibrated modifying the particles and flat-joint effective moduli (E^* and $\overline{E^*}$). Finally, the UCS (σ_c) is adjusted by tuning the cohesion (c), and tensile strength (σ_t), of the flat-joint.

On the other hand, the calibration of the SJCM parameters –i.e., the smooth-joint's normal and shear stiffnesses

($k_{n\,SJ}$ and $k_{s\,SJ}$); and its coefficient of friction ($\mu_{\,SJ}$)– were carried out through numerical direct shear tests on DEM^{2D} against the laboratory results of direct shear test of unbonded (i.e., with $c = 0$) rock-concrete planar interfaces under different normal stresses. To do that, the numerical samples for direct shear tests are generated using the Shear Box Genesis (SBG) method proposed by Bahaaddini et al. (2013). Next, the numerical joint normal stiffness ($K_{n\,DEM}$) is calibrated against the laboratory normal stiffness ($K_{n\,lab}$) through a normal deformability test on planar joints, in which the value of $k_{n\,SJ}$ is adjusted. Finally, the joint shear stiffness ($K_{s\,DEM}$) and the coefficient of friction (μ_{DEM}) are calibrated by trial and error adjusting the value of $k_{s\,SJ}$ and $\mu_{\,SJ}$ to reproduce the behaviour of laboratory shear tests (i.e., the shear stiffness, $K_{s\,lab}$, and the peak shear strength measured in the laboratory). Additional details of this methodology are available in Gutiérrez-Ch et al., (2018); and Bahaaddini et al., (2013). The calibrated FJCM and SJCM parameters are listed in Table 1 and Table 3, respectively. The numerical results of DEM^{2D} models and laboratory tests are presented in Table 2 and Table 3 indicating a good correlation between both approaches.

Table 1. Micromechanical properties fitted from the UCS tests employed in the calibration of intact material models.

Particle micromechanical properties	sandstone-S3	concrete
E^*(GPa)	1.90	27.00
$k^* = k_n/k_s$	1.45	2.75
Friction angle, ∅ (º)	35	30
Ball density, $\rho(kg/m^3)$	2550	2500
Minimum radius, R_{min} (mm)	1.0	0.8
R_{max}/R_{min}	1.4	1.5
Flat-joint micromechanical properties		
$\overline{E^*}$(GPa)	1.90	27.00
$\overline{k^*}$	1.45	2.75
c (MPa)	7.90	13.55
σ_t (MPa)	3.5	6.0

Table 2. Macromechanical properties for the UCS tests employed in the calibration of intact material model (laboratory data from Gu et al., 2003).

Sample	Macro-properties	Laboratory	PFC^{2D}
		Ave.	Ave.
Sandstone-S3	σ_c (MPa)	21.77	21.65
	E (GPa)	3.25	2.32
	ν	0.10	0.11
Concrete	σ_c (MPa)	40	39.87
	E (GPa)	29.95	30.08
	ν	0.20	0.20

3.2. *Generation of the samples to simulate rock-socketed piles*

An idealized sub-surface profile of a rock socket, and the associated DEM^{3D} model developed to represent it, are presented in Fig. 3. The nominal socket radius (R) and the nominal socket length (L) are, 0.4 m and 0.8 m, respectively. And, to minimize the computational cost, note that a 45-degree angle portion of the pile (instead of the whole pile) was considered, and that pressure loads (instead of actual bodies) are employed to simulate the self-weight of the pile (Q_1) and the overlying soil stratum (Q_2).

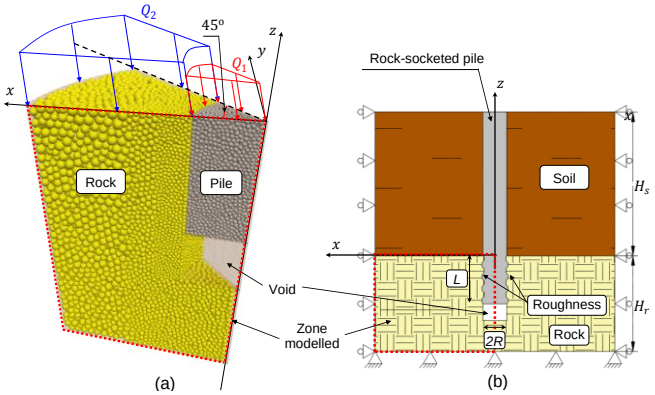

Fig. 3 (a) rock-socketed pile model in DEM^{3D}, (b) idealized sub-surface profile and nomenclature.

Table 3. a) Fitted parameters (with DEM^{2D} models) of SJCM on planar interface employed for validation, (b) comparison of joint macroscopic parameters for direct shear tests with DEM^{2D} results and measured in the laboratory by Gu et al. (2003).

a) Micromechanical parameters of the SJCM	Sandstone(S3)-concrete)	
Joint normal stiffness, $k_{n\,SJ}$ (MPa/mm)	10	
Joint shear stiffness, $k_{s\,SJ}$ (MPa/mm)	2	
Joint coefficient of friction, μ_{SJ} (tan ∅ (º))	0.70	
b) Macroproperties of the joint	Laboratory from Gu et al. (2003)	(PFC^{2D})
System normal stiffness, K_n, (MPa/mm)	-	10.30
System shear stiffness, K_s, (MPa/mm)	1.37	1.36
Friction angle, tan ∅ (º)	34.96	34.99

In addition, to obtain different degrees of socket roughness, the pile-rock interface was simulated by sinusoidal surfaces with asperity amplitudes of 0, 10, 20 and 40 mm, and the wavelength was 250 mm in all models (according to O'Neill et al., 1996). The four rock-socketed pile models were denoted for different roughness factor (RF = 0.000, 0.025, 0.050 and 0.106, see Fig. 4) defined by Horvath et al. (1983) as follows:

$$RF = \frac{h_m L_t}{RL} \tag{2}$$

where h_m is average height of asperities, R is the nominal socket radius, L_t is the total travel distance along the socketed wall, and L is the nominal socket length.

The methodology to simulate rock-socketed piles in DEM^{3D} model developed herein can be summarized as follows:

(a) *Initial particle assembly of rock and pile bodies:* the 3D model consisting of several frictionless walls is filled with an assemble of randomly placed particles. To reduce computation cost, the rock body was discretized into three zones using "secondary walls" (Fig. 5a), and having the smallest particles at the pile-rock interface. Particle radii satisfy a uniform distribution bounded by R_{min} and R_{max} (Table 4) (Fig. 5a).

(b) *Application of an isotropic initial stress:* first, the secondary walls are deleted. Next, "measurement regions" –blue spheres in Fig. 5b– are installed inside the pile and rock bodies and the normalized difference $\sigma_{step} = ((\sigma_o^c - \sigma_o)/\sigma_o^c)$ within each "measurement region" is computed for each step. If $\sigma_{step} \geq \sigma_{tol}$, the radii of all particles are iteratively changed, otherwise, the process finishes (according to Bahaaddini et al., 2013 and Gutiérrez-Ch et al., 2018, $\sigma_o^c \cong 1\%$ of the uniaxial compressive strength and $\sigma_{tol} = 0.5$ are used). Thus, a better distribution of contacts is obtained and the magnitude of the locked-in forces are reduced.

(c) *Elimination of floating particles:* "floating" particles with less than three contacts can appear during the previous steps (purple spheres in Fig. 5c), and the radii of floating particles are increased until all particles away from the specimen boundaries have at least three contacts.

(d) *Application the FJCM and SJCM:* first, the flat-joint contacts (with their corresponding parameters) are installed separately in rock and pile bodies. Next, the wall corresponding to the intended contact at the pile-rock interface is removed, and the SJCM is applied to particles in contact with the pile-rock surface. The micro-properties used for FJCM and SJCM were listed in Table 1 and Table 3.

(e) *Initialization of in situ stress and boundary conditions:* a gravity load to induce in situ stress (self-weight) was applied. In addition, pressure loads of (i) the self-weight of the pile ($Q_1 = 0.125$ MPa) and (ii) the overlying soil stratum ($Q_2 = 0.1$ MPa) are applied on the wall head pile and on the wall rock, respectively (see Fig. 3a).

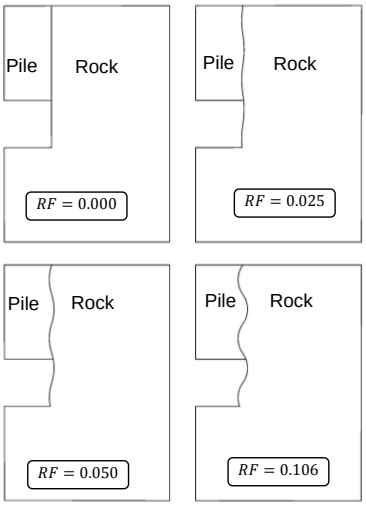

Fig. 4 2D view of the socket roughness at the pile-rock interfaces for models in DEM[3D].

Table 4. Particle size distributions in the numerical models of rock-socketed piles testing.

		Minimum radius, R_{min} (cm)	R_{max}/R_{min}
Rock	Zone 1	1.00	1.5
	Zone 2	1.50	1.5
	Zone 3	2.25	1.5
Pile	Zone 1	1.00	1.5

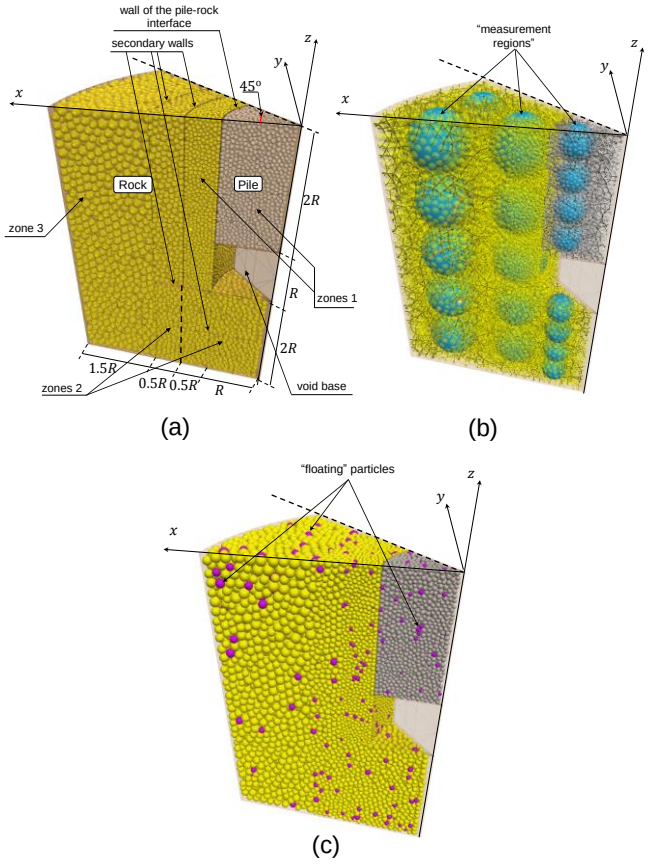

Fig. 5. (a) rock-socketed pile container and initial particle assembly (b) contact-force distribution after isotropic stress installation (black lines represent contact-force intensity and blue spheres represent the "measurement regions"), (c) detection of floating particles (purple balls represent floating particles).

Finally, to conduct the numerical rock-socketed pile testing, the wall at the base of the pile body is removed, the displacements of the boundary walls are restraint and an axial velocity (V_z) that is low enough to ensure that the model specimens remain in quasi-static equilibrium (for example 0.05 m/s) is applied on the pile wall head. The pile head movement (δ) and axial force (P) are obtained, respectively, through the axial displacements and force reaction recorded at the wall head pile.

4. RESULTS

4.1. Load-settlement response

The load-settlement curves from the DEM[3D] simulations of four piles socketed into sandstone-S3 (with different roughness profiles) are shown in Fig. 6. All analyses were

conducted until a limit socket head settlement (δ) of 10% of the socket diameter ($0.1D$) is reached. Results in Fig. 6 show that socket roughness is an important factor that significantly increases the load capacity and stiffness of rock-socketed piles: for instance, the model with $RF = 0.050$ supported a working load 2.1 times higher than that supported by the model with $RF = 0.025$, for an identical pile head settlement of $0.02D$ (1.6 cm).

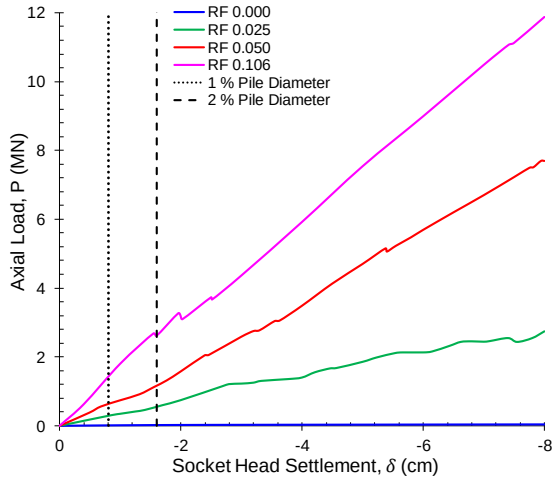

Fig. 6. Load-settlement responses of rock-socketed piles on sandstone-S3 with different roughness computed with DEM[3D].

4.2. *Average side shear resistance*

The computed curves relating f_{ave} and δ for rock sockets on sandstone-S3 with different roughness are presented in Fig. 7. As it can be seen the average side shear resistance increases as the roughness of the interface increases; for instance, f_{ave} of the models with $RF = 0.025$ is about 2 times higher than that obtained with $RF = 0.010$. This can be explained by the fact that the pile-rock interface with higher RF produces more dilation and normal stiffness (see e.g., Seol and Jong, 2007 and Gutiérrez-Ch et al., 2018).

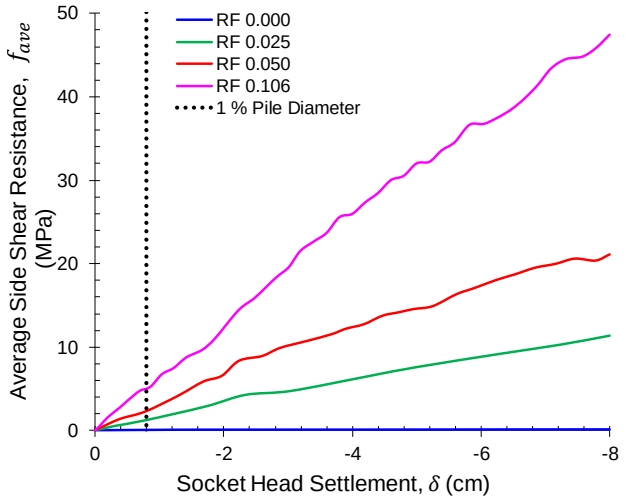

Fig. 7. Average side shear resistance (f_{ave}) versus socket head settlement (δ) on sandstone-S3.

4.3. *A factor $\alpha_{RF,0.01D}$ for side shear resistance prediction considering socket roughness*

The results of the DEM[3D] numerical model are employed to develop a preliminary factor $\alpha_{RF,0.01D} = f_{ave,0.01D}/\sqrt{\sigma_c}$ (see Fig. 8), to estimate the average side shear resistance in the type of piles drilled in sandstone considered herein, and for a socket head settlement of $0.01D$. The approach considers (i) the roughness at the rock-concrete interface, through the roughness factor RF; and (ii) the uniaxial compressive strength, σ_c, of the weaker material (intact rock or pile). Contrary to other previous approaches published in the literature (see e.g., Horvath et al. 1983), the proposed approach accounts for the socket roughness in its estimation of α. Considering the DEM[3D] numerical results, a value of $\alpha_{RF,0.01D} = 10RF$ seems, in this case, as an adequate approximation for a preliminary average side shear resistance prediction.

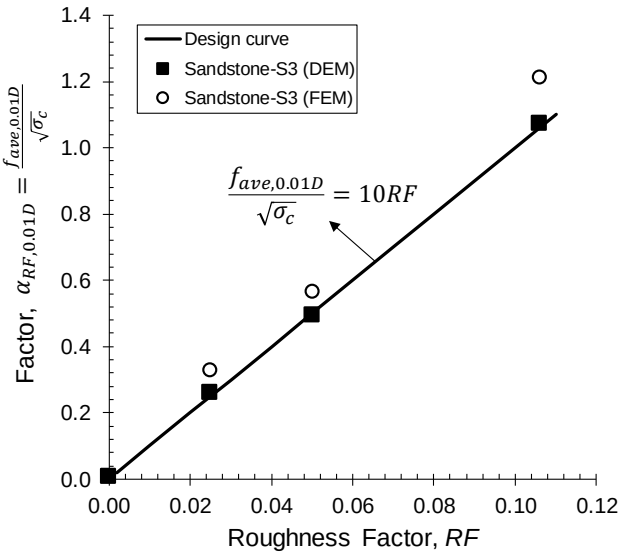

Fig. 8. Factor $\alpha_{RF,0.01D}$ for average side shear resistance $f_{ave,0.01D}$ prediction considering a socket head movement equivalent to $0.01D$.

To compare the behaviour of the preliminary factor $\alpha_{RF,0.01D}$ proposed herein, Finite Element Method (FEM) models were performed using Abaqus commercial code (Smith, 2009). To do that, axisymmetric models with the geometry presented in Fig. 4, and with $RF = 0.025$, 0.050 and 0.106 were used. The pile was modeled as elastic, using the macro-properties listed in Table 2. To reproduce the rock behaviour, an elastic-perfectly plastic model with the Mohr-Coulomb yield criterion was used. The rock elastic parameters are listed in Table 2, and the cohesion and friction angle were 2.2 MPa and 35°, respectively. At the pile-rock interface, the basic Coulomb friction model with a coefficient of friction of 0.7 was used. The loads applied and the boundary conditions were equivalent to those employed in the DEM models. As an initial step, the in situ stress was applied. Next, the geostatic step was conducted to reach the

equilibrium between the in situ stress and the applied loads and boundary conditions (Smith, 2009). Finally, the pile head was axially loaded with a displacement controlled procedure.

The average side shear resistance computed from the FEM models for a socket head settlement of $0.01D$ and normalized by $\sqrt{\sigma_c}$ are plotted in Fig. 8. As it can be seen, the FEM results are similar to those obtained with DEM models, suggesting that the factor $\alpha_{RF,0.01D}$ can be employed for a preliminary side shear resistance estimation. Additional research is being currently conducted to assess the adequacy of this approach to sockets in other types of rock.

5. CONCLUSIONS

The degree of socket roughness has a significant impact on the load-settlement behaviour of rock-socketed piles, as well as on the side shear resistance. This papers demonstrates that discrete numerical models constructed with DEM[3D] can be employed to (i) reproduce the load-settlement behaviour of rock sockets with different roughness and (ii) to estimate their side shear resistance.

Finally, the numerical results of this research suggest that a new empirical factor, $\alpha_{RF,0.01D} = f_{ave,0.01D}/\sqrt{\sigma_c}$, can be employed to estimate preliminary the average side shear resistance of sockets in the sandstone rock considered herein, and for an approximate socket head settlement of 1% of the socket diameter. Results suggest that a value of $\alpha_{RF,0.01D} = 10RF$ could be an adequate relationship to be employed for preliminary design of rock-socketed piles in the sandstone considered herein; however, further analyses are being conducted to further validate the approach in other types or rocks. The results of such research will be presented elsewhere.

ACKNOWLEDGEMENTS

The first author has received during 2018 the scholarship for PhD research provided by the José Entrecanales Ibarra Foundation. This support is gratefully acknowledged.

REFERENCES

1. Bahaaddini, M., Sharrock, G., and Hebblewhite, B. K. 2013. Numerical direct shear tests to model the shear behaviour of rock joints. *Comput. Geotech.* 51: 101–115.
2. Castro-Filgueira, U., Alejano, L., Arzúa, J., Ivars, D.M., 2017. Sensitivity analysis of the micro-parameters used in a PFC analysis towards the mechanical properties of rocks. *Procedia Eng.* 191, 488-495.
3. Gu, X. F., Seidel, J. P., and Haberfield, C. M. 2003. Direct shear test of sandstone-concrete joints. *Int. J. Geomech.* 3, 21–33.
4. Gutiérrez-Ch, J. G., Senent, S., Melentijevic, S., and Jimenez, R. 2018. Distinct element method simulations of rock-concrete interfaces under different boundary conditions. *Eng. Geol.* 240, 123–139.
5. Haberfield, C. M. 2013. Performance of footings in rock based on serviceability. *Australi. Geomech. J.* 48(1), 1–49.
6. Horvath, R. G., Kenney, T. C., and Kozicki, P. 1983. Methods for improving the performance of drilled piers in weak rock. *Can. Geotech. J.* 20(4), 758–772.
7. Itasca Consulting Group Inc. 2014. PFC Manual, Version 5.0. (Minneapolis, Minnesota).
8. Ivars, D. M., Potyondy, D. O., Pierce, M., and Cundall, P. A. 2008. The smooth-joint contact model. In *Proceedings of the 8th. World Congress on Computational Mechanics (WCCM8) - 5th. European Congress on Computational Methods in Applied Sciences. and Engineering (ECCOMAS). Venice, Italy, 30-June–5-July*.
9. Ivars, D. M., Pierce, M. E., Darcel, C., Reyes-Montes, J., Potyondy, D. O., Young, R. P., and Cundall, P. A. 2011. The synthetic rock mass approach for jointed rock mass modelling. *Int. J. Rock Mech. Min. Sci.* 48, 219–244.
10. Melentijevic, S., and Olalla, C. 2014. Different FEM models for simulation of the Osterberg load test in rock shafts. *ISRM Regional Symp. EUROCK 2014. London, United Kingdom*.
11. Nam, M. S., and Vipulanandan, C. 2008. Roughness and unit side resistances of drilled shafts socketed in clay shale and limestone. *J. Geotech. Geoenviron. Eng.* 134(9), 1272–1279.
12. O'Neill, M. W., Townsend, F. C., Hassan, K. M., Buller, A., and Chan, P. S. 1996. Load transfer for drilled shafts in intermediate geomaterials. U.S. Department of Transportation, FHWA-RD- 95–172, Final Report.
13. Pells, P. J. N., Rowe, R. K., and Turner, R. M. 1980. "An experimental investigation into shear for socketed piles in sandstone." In *Proceedings of the International Conference on Structural Foundations on Rock, 1, 291–302. Sydney, Australia, 7–9 May*.
14. Potyondy, D. O. 2012. A flat-jointed bonded-particle material for hard rock. *46th US Rock Mechanics/Geomechanics Symposium. Chicago, Illinois*.
15. Potyondy, D. O. (2015). The bonded-particle model as a tool for rock mechanics research and application: current trends and future directions. *Geosyst. Eng.* 18, 1–28.
16. Rezazadeh, S., and Eslami, A. 2017. Empirical methods for determining shaft bearing capacity of semi-deep foundations socketed in rocks. *Int. J. Rock Mech. Geotech. Eng.* 9(6), 1140–1151.
17. Seidel, J. P., and Haberfield, C. M. 1995. The axial capacity of pile sockets in rocks and hard soils. *Ground Eng*. 28(2), 33–38.

18. Seidel, J. P., and Collingwood, B. (2001). A new socket roughness factor for prediction of rock socket shaft resistance. *Can. Geotech. J.* 38(1), 138–153.

19. Seo, H., Prezzi, M., and Salgado, R. 2013. Instrumented static load test on rock-socketed micropile. *J. Geotech. Geoenviron. Eng.* 139(12), 2037-2047.

20. Seol, H. I., and Jeong, S. S. (2007). Shaft resistance characteristics of rock-socketed drilled shafts based on pile load tests. *J. Korean Geotech. Soc.* 23(9), 51–63.

21. Smith, M. (2009). ABAQUS/Standard User's Manual, Version 6.12. Providence, RI: Simulia.

22. Williams, A. F., and Pells, P. J. N., 1981. Side resistance in sandstone, mudstone, and shale. *Can. Geotech. J.* 18(4), 502–513.

23. Zhang, L. (2004). Drilled shafts in rock: analysis and design. London (UK): Balkema.